Distinct Roles of Myosins in *Aspergillus fumigatus* Hyphal Growth and Pathogenesis

Running title: Characterization of myosins in *Aspergillus fumigatus*

Hilary Renshaw[1], José M. Vargas-Muñiz[1], Amber D. Richards[2], Yohannes G. Asfaw[3], Praveen R. Juvvadi[2], William J. Steinbach[1,2]#

[1]Department of Molecular Genetics and Microbiology, Duke University Medical Center, Durham, NC, USA, [2]Division of Pediatric Infectious Diseases, Department of Pediatrics, Duke University Medical Center, Durham, NC, USA, [3]Division of Laboratory Animal Resources, Duke University Medical Center, Durham, NC, USA

#Address correspondence to William J. Steinbach, bill.steinbach@duke.edu

ABSTRACT

Myosins are a family of actin-based motor proteins found in many organisms and categorized into classes based on their structure. Class II and V myosins are known to be important for critical cellular processes, including cytokinesis, endocytosis, exocytosis, and organelle trafficking in the model fungi *Saccharomyces cerevisiae* and *Aspergillus nidulans*. However, myosins' roles in the growth and virulence of the pathogen *Aspergillus fumigatus* are unknown. We constructed single and double deletion strains of the class II and class V myosins in *A. fumigatus* and found that while the class II myosin (*myoB*) is dispensable for growth, the class V myosin (*myoE*) is required for proper hyphal extension; deletion of *myoE* resulted in hyper-branching and loss of hyphal polarity. Both *myoB* and *myoE* are necessary for proper septation, conidiation, and conidial germination, but only *myoB* is required for conidial viability. Infection with the Δ*myoE* strain in the invertebrate *Galleria mellonella* model and also in a persistently immunosuppressed murine model of invasive aspergillosis resulted in hypovirulence while analysis of bronchoalveolar lavage fluid revealed that TNF-α release and cellular infiltration was similar compared to the wild-type strain. The Δ*myoE* strain showed fungal growth in the murine lungs, while the Δ*myoB* strain exhibited little fungal burden, most likely due to the reduced conidia viability. These results show, for the first time, the important role these cytoskeletal components play in the growth and disease of a known pathogen, prompting future studies to understand their regulation and potential targeting for novel antifungal therapies.

INTRODUCTION

In filamentous fungi, the actin cytoskeleton is critical for a myriad of important cellular functions, including cytokinesis, hyphal tip growth, endocytosis, and exocytosis (1-7). Myosins are involved in many of these roles by their interaction with actin microfilaments. The number of myosins vary greatly between organisms; however, fungi contain relatively few myosins in comparison to humans (8). Myosins have been studied in the model fungi *Saccharomyces cerevisiae* and *Aspergillus nidulans*, (1, 3, 9-15) but not in the pathogen *Aspergillus fumigatus*. *S. cerevisiae* contains five myosin-encoding genes encompassing three classes (16-20), while the filamentous fungus *A. nidulans* possesses four classes of myosins: class I, class II, class V, and the fungal-specific class XVII, which contains a myosin motor head and a chitin synthase domain (1, 5, 14). The conventional myosins, class II myosins, have a role in cytokinesis through involvement in the cytokinetic actomyosin ring (CAR) (21). Deletion of the class II myosins in *Penicillium marneffei* and *A. nidulans* led to cytokinesis defects or septation failure (5, 22). In addition, mutants lacking the sole class II myosin in *A. nidulans* (MyoB) exhibited a lack of conidiation, extreme growth defects, and improper chitin deposition (5). Further supporting its role in septation, *A. nidulans* MyoB transiently localized to the septum as nodes or strings (5).

Class V myosins are vesicle transporters and important for maintaining cell polarity (5, 13, 19, 23, 24). *S. cerevisiae* genome encodes two class V myosins, one of which is essential (Myo2p) (18, 23). Mutation of *myo2* leads to enlarged and unbudded cells with an accumulation of secretory vesicles (19, 23). Similarly, deletion of the class V myosin in *Candida albicans* leads to unbudded large cells that do not form germ tubes or hyphae (25). Deletion of the class V myosin in the plant pathogenic fungus *Ustilago maydis* decreases virulence in maize plants (26). In *A. nidulans,* the sole class V myosin (MyoE) is not essential but is required for proper vesicle trafficking to the Spitzenkörper in an actin-dependent manner (5). The *A. nidulans* MyoE

64 localized to the Spitzenkörper, in dot-like structures throughout the hyphae, and transiently at the
65 septa under its native promoter (5, 7). However, under the control of a regulatable promoter,
66 MyoE was shown to localize stably to both sides of the septa (7). Deletion of *myoE* in *A.*
67 *nidulans* led to morphologically normal septa that were closer together (7); however, the function
68 of the class V myosin in this process is currently unknown. Myosins' known roles in critical
69 cellular processes, including hyphal tip growth and cytokinesis, make them likely crucial for
70 cellular functions related to pathogenesis.

71 Despite the established functions of myosins in other fungi, their roles in the pathogen *A.*
72 *fumigatus* have not been established. In this study, we characterized the class II (MyoB) and
73 class V (MyoE) myosins of *A. fumigatus* and their roles in hyphal growth and virulence by
74 generating single deletions of both *myoB* (Δ*myoB*) and *myoE* (Δ*myoE*) as well as a double
75 deletion strain (Δ*myoB* Δ*myoE*). While the deletion of *myoB* resulted in aberrant septation and
76 reduced conidiation, the deletion of *myoE* caused a significant growth defect, hyperseptation,
77 hyperbranching, loss of hyphal polarity, and a loss of conidiation. Deletion of both *myoB* and
78 *myoE* resulted in a more severe phenotype. The Δ*myoE* strain displayed attenuated virulence in a
79 *Galleria mellonella* model and in an intranasal murine model of invasive aspergillosis and
80 similarity in TNF-α release and cellular infiltration in comparison to infection with the wild-type
81 strain. Although the Δ*myoB* strain showed decreased mortality in both animal models and a
82 significant reduction in TNF-α release, this is most likely due to the reduced conidia viability and
83 therefore decreased fungal burden.

84

85 **MATERIALS AND METHODS**

Strains, media, and culture conditions. Strains used in this study are listed in Table 1. The *A. fumigatus akuB*^{KU80} or the *akuB*^{KU80} *pyrG*$^{-}$ uracil/uridine auxotrophic strains were used for deletion analyses and the *A. fumigatus akuB*^{KU80} strain was used as the wild-type reference strain. Cultures were grown on glucose minimal media (GMM) supplemented with 5 mM uracil and 5 mM uridine (GMM+UU) at 37°C, except where otherwise specified. *Escherichia coli* DH5α competent cells were used for cloning.

Construction of myosin deletion and GFP-tagged strains. Primers used are listed in Table S1. Both the Δ*myoB* and the Δ*myoE* strain were generated by replacing each gene with *pyrG* from *Aspergillus parasiticus*. Approximately 1 kb upstream and downstream of each gene was PCR amplified from *A. fumigatus* AF293 genomic DNA and cloned into the pJW24 vector (27). Resulting plasmids were linearized with SalI and SacI to obtain the deletion cassette (approximately 5.5 kb for *myoB* and 5.2kb for *myoE*) and transformed into *akuB*^{KU80} *pyrG*$^{-}$ auxotrophic strain as previously described (27). Transformants were selected for growth in the absence of uracil/uridine. To construct the double deletion strain, the pBlue-phleo plasmid was constructed by digesting pBlueScriptII and pUCnGPhleo (28) with HindIII and ligating the *ble* cassette into pBlueScript II. Approximately 1 kb upstream and downstream sequences of *myoE* were PCR amplified from AF293 genomic DNA and cloned into pBlue-phleo. Resulting plasmid was used as a template for final PCR amplification for transformation. The 5 kb PCR product was transformed into the Δ*myoB* strain and transformants were selected in the presence of phleomycin (125 μg/ml). Deletions were confirmed by PCR and/or Southern analysis. The *myoB-egfp* expression strain was generated by cloning approximately 1 kb of partial *myoB gene* and 1 kb of *myoB* terminator sequence into the pUCGH vector (29). The resulting plasmid was linearized with KpnI and HindIII and transformed into the *akuB*^{KU80} strain. The *myoE-egfp* strain

was generated by cloning approximately 1 kb of partial *myoE* gene and 1 kb of *myoE* terminator sequences into pUCGH. The resulting plasmid was linearized with KpnI and XbaI and transformed into the *akuB*^{KU80} strain. Transformants were selected by growth in the presence of hygromycin B (150 µg/ml).

Radial growth, conidial harvesting and quantification. Conidia (10^4) were inoculated on GMM+UU or sorbitol minimal media (SMM) agar, incubated at 37°C, and radial growth measured every 24 h for 5 days. To quantify conidial production, 10^4 conidia were inoculated onto GMM+UU or SMM agar, incubated at 37°C for 5 days, harvested in 10 ml 0.05% Tween-80 and quantified using a hemacytometer as previously described (30). All assays were performed in triplicate. The mean growth rates for each of the strains were compared statistically by Student's *t* test using GraphPad Prism (San Diego, CA). To obtain conidia for experimentation, conidia (10^4) were inoculated onto SMM, grown for 5 days at 37°C with the exception of the Δ*myoB* Δ*myoE* strain which was grown for 14 days to allow for sufficient conidia production, and harvested in 10 ml 0.05% Tween-80. Harvested conidia were diluted and stored at 4°C in water.

Fluorescence and Transmission electron microscopy. For fluorescence microscopy, conidia (10^4) were inoculated and cultured for 18 h at 37°C in 60x15 mm petri dishes containing coverslips (22 x 40 mm; No. 1) immersed in 5 ml GMM liquid media. Strains were observed using an Axioscop 2 plus microscope (Zeiss) equipped with AxioVision 4.6 imaging software.

For transmission electron microscopy (TEM) of hyphae, conidia were inoculated into 10 ml GMM and incubated at 37°C for 24 h to generate hyphae. For TEM of conidia and hyphae, samples were centrifuged at 2000 rpm for 5 min and supernatant removed. Samples were washed

twice with PBS for 10 min, stained for one hour with osmium tetroxide, and washed twice with PBS and once with 0.1N acetate buffer for 10 min. Samples were stained with 0.5% uranyl acetate for 1 h, and washed twice for 10 min using 0.1N acetate buffer, and dehydrated using serial washes of 30%, 50%, 70%, 90% and 100% ethanol twice for 10 min at each concentration. Samples embedded using the SPURR Low Viscosity Embedding Kit were thin sectioned and stained using 1% uranyl acetate and 0.4% lead citrate. Hyphae were visualized using an accelerating voltage of 80 kV on a FEI Tecnai G^2 Twin.

Aniline blue, Calcofluor white staining, and apical/subapical compartment measurements. Conidia (10^4) of each strain were cultured in 60x15 mm petri dishes with coverslips immersed in 5 ml of GMM+UU broth and incubated for 18 h at 37°C (28). For aniline blue staining, coverslips were rinsed with GMM+UU broth, inverted over 500 µl of aniline blue stain, and incubated for 5 min at 25°C. Coverslips were rinsed briefly with GMM+UU broth and observed by fluorescence microscopy. For calcofluor white staining, coverslips were washed in 50 mM PIPES (pH 6.7) for 5 min, fixed in 8% formaldehyde for 1 hour at 25°C, washed twice in 50 mM PIPES (pH 6.7) for 10 min at 25°C, and then treated with 100 µg/ml RNase for 60 min at 37°C. Samples were then stained with 1 µg/ml calcofluor white in 500 µl of PIPES (pH 6.7) for 5 min and visualized under the fluorescent microscope.

To determine the apical and subapical compartment measurements, conidia (10^4) were cultured on coverslips immersed in 5 ml of GMM+UU broth, incubated for 18 h at 37°C (28), then stained with aniline blue as previously described and visualized using fluorescent microscopy. The apical compartment was measured from the apex of the hyphae to the apical septum. The subapical compartment was measured from the apical septum to the subapical septum. Statistical

153 analysis was performed using a Student's *t* test comparing wild-type strain apical vs. Δ*myoE*
154 strain apical length and wild-type strain subapical vs. Δ*myoE* strain subapical length.

155 **Antifungal susceptibility testing.** Conidia (10^4) were inoculated on GMM+UU agar
156 supplemented with either caspofungin (1 or 4 μg/ml) or nikkomycin Z (2 μg/ml) and growth
157 visualized after 5 days at 37°C. For liquid culture, conidia (100 μl of 2 x 10^4) were inoculated
158 into RPMI media according to CLSI standards and supplemented with the appropriate
159 concentrations of caspofungin and growth monitored for 48 h to determine the minimum
160 effective concentration (MEC) of the anti-cell wall agent on the strains (31, 32).

161 ***Galleria mellonella* and murine invasive aspergillosis animal models.** As initial virulence
162 screening in the invertebrate *Galleria mellonella* invasive aspergillosis infection model, 20
163 larvae were infected with 5 μl of 1 x 10^8 conidia/ml suspension. Infected larvae were incubated
164 at 37°C and survival scored daily for 5 days (27). For the murine model of invasive aspergillosis,
165 male CD1 mice (Charles River Laboratories, Raleigh, NC) were immunosuppressed with
166 cyclophosphamide (175 mg/kg intraperitoneally on day -2 and +3) and triamcinolone acetonide
167 (40 mg/kg subcutaneously on days -1 and + 6) and intranasal infection of 20 mice per strain was
168 performed on day 0 with 40 μl of 10^8/ml conidia; mice were monitored daily for survival for 14
169 days (33). Survival for the invertebrate and murine models was plotted on a Kaplan-Meier curve
170 with log rank pair-wise comparison. Statistical significance was defined as a two-tailed *P* value
171 of <0.05.

172 **Histopathology of murine lungs.** Three additional mice per strain were examined for
173 histological examination. Mice were euthanized at day +3 after infection, lungs harvested, and

tissue (5 µm sections) stained with Gomori's methenamine silver stain and hematoxylin and eosin stain (27).

Bronchoalveolar lavage, ELISA, flow cytometry analysis

Five additional mice per strain were immunosuppressed and infected as described above with water being used as mock. On day +3, bronchoalveolar lavage fluid (BALF) was collected by instilling the lungs with 5 ml PBS containing 0.05M EDTA. The first 1 ml collected was centrifuged and the supernatant removed for TNF-α quantification by ELISA. The cell pellet was added to the other 4 ml BALF collected. TNF-α release was measured using the Mouse TNF-α ELISA MAX Standard kit (BioLegend) following the manufacturer's instructions. For flow cytometric analysis of BALF cells, single cell BALF suspensions were washed and stained with antibodies specific for the following cell surface markers: CD115 and Ly6C (eBioscience, San Diego, CA), CD11b, CD11c, CD24, CD31, IA/IE, Ly6G, and Siglec-F (BD Biosciences, San Jose, CA), and CD3, CD45, CD64, CD103, B220 and F4/80 (Biolegend, San Diego, CA). One channel was used to detect autofluorescence. In addition, Zombie Yellow Live/Dead (Biolegend, San Diego, CA) was used to exclude dead cells. Data were collected with a BD LSRII flow cytometer and analyzed with Flowjo software. Single cells were identified using forward and side scatter, dead cells were excluded, and leukocytes were identified as $CD45^+$ cells. Neutrophils were identified as $CD45^+$ $Ly6G^+$ cells, and alveolar macrophages were identified as being $CD45^+$, $Ly6G^-$, $CD64^+$, $Siglec\text{-}F^+$ cells. For ELISA and flow cytometry, statistical significance of $p<0.05$ was determined using an unpaired *t* test comparing the wild-type strain to the deletion strains.

196 **Germination and conidial viability.** Conidia (~100) were inoculated into 5 ml GMM in 60x15
197 mm petri plates in triplicate and incubated at 37°C. Fifty conidia were quantified per plate every
198 hour for 18 h, then again at 24 h, 36 h, and 48 h time points for the double deletion strain using a
199 Nikon Diaphot Phase Contrast microscope. Conidia were considered germinated when a germ
200 tube was visible. The statistical differences for the groups at the 18-h time point were determined
201 pairwise by the chi-square test.

202 To obtain conidia for viability staining, conidia (10^4) were inoculated onto SMM, grown for 5
203 days at 37°C and harvested in 10 ml water or PBS. Harvested conidia were diluted and stored at
204 4°C in water or PBS for 4 days. For viability staining, conidia (10^4) were centrifuged at 13,000
205 rpm for 2 min and supernatant removed. Bis-(1,3-dibutylbarbituric acid) trimethine oxonol
206 (DiBAC) (2 µg/ml in 100mM MOPS 7) was added to conidia to stain them, samples vortexed
207 and incubated in the dark at room temperature for 1 h, then centrifuged at 13,000 rpm for 2 min,
208 supernatant removed, and conidia washed twice with 100 mM MOPS, pH 7.0 (34).
209 Carboxyfluorescein diacetate (CFDA) (50 µg/ml in 100mM MOPS 3) was added to conidia,
210 samples vortexed and incubated in the dark for 45 min at 37°C with gentle agitation. Stained
211 conidia were visualized using an Axioscop 2 plus microscope (Zeiss) with the GFP filter. Fifty
212 conidia were counted three times per strain and marked as viable or inviable. Statistical
213 significance of $p<0.05$ was determined using an unpaired *t* test comparing the wild-type strain to
214 the deletion strains or multiple *t* tests to compare water vs. PBS harvested conidia.

215

216 **RESULTS**

Deletion of *myoB* or *myoE* result in abnormal colony morphology, conidiation defects, septation, and cell wall component localization. To investigate the role of myosins in *A. fumigatus,* we generated single deletion strains (Δ*myoB* and Δ*myoE*) and a double deletion strain (Δ*myoB* Δ*myoE*) (Figure S1A and S1B). While the Δ*myoB* strain showed radial growth comparable to the wild-type strain, the Δ*myoE* strain and the Δ*myoB* Δ*myoE* strain each showed a significant defect in radial growth ($p<0.000001$ for both at day 5) (Fig. 1D). Under differential interference contrast microscopy, the Δ*myoE* strain and the Δ*myoB* Δ*myoE* strain displayed hyperbranching and loss of polarity, (Fig. 1A and 1B) while the Δ*myoB* strain appeared normal.

All three myosin deletion strains grew as white colonies on glucose minimal media (GMM), which could indicate a lack of conidiation (Fig. 1A and 1B). Quantification of conidial production showed that the Δ*myoB* strain resulted in a > 99% decrease in conidiation ($p<0.0001$) when compared to the wild-type strain grown in GMM. The Δ*myoE* and Δ*myoB* Δ*myoE* strains completely lacked conidia. The conidiation defect was partially remediated in each mutant strain in the presence of sorbitol (data not shown); however, the remediated Δ*myoB* Δ*myoE* strain produced conidia only after 14 days of growth. Quantification of conidial production when grown in the presence of sorbitol showed that the Δ*myoB* strain produced equal number of conidia as the wild-type strain ($p>0.05$), while the Δ*myoE* strain exhibited a nearly 75% decrease ($p<0.01$) and the Δ*myoB* Δ*myoE* strain exhibited a > 80% decrease ($p<0.01$) in comparison to wild-type strain.

Previous studies in *A. nidulans* showed that deletion of *myoB* or *myoE* affected septation, therefore we used aniline blue, which selectively stains cell wall β-(1,3)-glucan, and found that deletion of *myoB* nearly abolished all septation, and any septa that could be visualized possessed either central or lateral defects in septation leading to abnormal septal closure. This included

240 septa extending from both sides of the hyphae but not meeting centrally or septa only extending
241 from one side (Fig. 1A). Conversely, deletion of *myoE* resulted in hyperseptation but with
242 normal septal morphology. However, the double deletion strain showed aberrantly formed,
243 incomplete septa and irregular β-(1,3)-glucan deposition (Fig. 1B). The myosin deletion strains
244 were also stained with calcofluor white to visualize chitin. The Δ*myoB* strain showed irregular
245 accumulation of chitin, as was observed with β-(1,3)-glucan (Fig. 1A). In contrast, the Δ*myoE*
246 strain showed complete septa but small concentrated patches of chitin near some septal sites
247 (Fig. 1A). Collectively, these data indicate that both *myoB* and *myoE* are important for proper
248 assembly of cell wall components at the septum.

249 To better characterize the abnormal septa, transmission electron microscopy (TEM) was
250 performed on the wild-type and deletion strains (Fig. 1C). We visualized malformed septa in the
251 Δ*myoB* strain and also noted that the Δ*myoB* septa were thicker than wild-type septa. Although
252 the Δ*myoE* strain showed a severe radial growth defect when compared to the wild-type strain,
253 its septa appeared normal. However, in the Δ*myoB* Δ*myoE* strain, no intact hyphae were present.
254 It is possible that sample preparation procedure for TEM may have caused hyphal lysis, but the
255 mislocalization of β-(1,3)-glucan and lack of septation in this strain suggest cell wall defects. It
256 remains unclear whether the β-(1,3)-glucan patches seen with aniline blue staining are
257 improperly formed septa or mislocalized β-(1,3)-glucan.

258 Although TEM analysis did not show any defects in septal morphology in the Δ*myoE* strain, the
259 deletion resulted in hyperseptation. To quantify this, we measured the apical and subapical
260 hyphal compartments. Deletion of *myoE* resulted in a 2-fold decrease in apical compartment size
261 and in subapical compartment size compared to the wild-type strain ($p<0.001$), indicating that
262 *myoE* is required for proper septal spacing (data not shown).

263

264 **Deletion of *myoB* and double deletion of *myoB* and *myoE* results in increased sensitivity to**
265 **cell wall stressors.** To experimentally examine if the lack of septation and mislocalization of
266 cell wall components in the mutant strains may be due to defective cell wall biosynthesis, we
267 treated the myosin deletion strains with anti-cell wall agents. In comparison to the wild-type
268 strain, the Δ*myoB* strain was more susceptible to the β-glucan synthase inhibitor caspofungin, but
269 not to the chitin synthesis inhibitor nikkomycin Z (Fig. 2A). The Δ*myoB* Δ*myoE* strain failed to
270 grow in the presence of caspofungin and was severely growth-inhibited with nikkomycin Z (Fig.
271 2A). The Δ*myoE* strain possessed equal growth in the presence or absence of anti-cell wall
272 agents (Fig. 2A). However, when grown in liquid culture supplemented with caspofungin, these
273 results slightly varied. MEC was determined to be 0.125 μg/ml for the Δ*myoE* strain and 0.25
274 μg/ml for the Δ*myoB* strain, both slightly lower than the wild-type strain (0.5 μg/ml). *A.*
275 *fumigatus* exhibits a phenomenon known as the paradoxical effect in which a wild-type strain
276 will be growth-inhibited at 0.5 to 2 μg/ml caspofungin but growth is remediated at 4 μg/ml
277 caspofungin. While this paradoxical effect remains for the Δ*myoB* strain in solid media (Figure
278 2A), it was not recapitulated in liquid media (Fig 2B). The Δ*myoB* strain exhibits little growth
279 from 0.5 μg/ml caspofungin up to 4 μg/ml caspofungin.

280

281 **MyoB and MyoE localize to the septum, while only MyoE localizes to the hyphal tip.**
282 Because our *A. fumigatus* myosin deletion strains morphological phenotypes were different from
283 those reported for *A. nidulans,* we speculated that there might be a variation in MyoB and MyoE
284 localization. To examine this, we GFP-labeled MyoB and MyoE each at the C-terminus and

characterized their localization after 18 h of growth under standard conditions. The MyoB-EGFP fusion protein localized throughout the hyphae in ring-like structures, seemingly at future sites of septation, and in motile dot-like structures in the cytoplasm (Fig. 3A). MyoB was also observed in dot-like structures at some but not all mature septa; however, this localization pattern was rare and disappeared rapidly. MyoE, under the control of its native promoter, localized stably at the septa as two bars on either side of septa, in nearly all hyphal tips, and in motile dot-like structures in the cytoplasm (Fig. 3B).

***myoE* is required for virulence in a *Galleria mellonella* and murine model of invasive aspergillosis.** Pathogenesis of filamentous fungi is generally facilitated by penetration of host tissue through radial hyphal extension. Considering the lack of hyphal extension in the Δ*myoE* strain, we hypothesized that this strain may exhibit attenuated virulence. We first screened the myosin deletion strains in the heterologous invertebrate host *Galleria mellonella.* As expected, the Δ*myoE* strain was hypovirulent, with a nearly 50% greater survival rate five days after infection ($p<0.0001$) compared to the wild-type strain (Fig. 4A). The Δ*myoB* strain was showed decreased mortality with a 40% greater survival rate ($p<0.001$) despite radial hyphal extension similar to the wild-type strain (Fig. 4A).

Following screening in the *Galleria* model, we utilized an intranasal murine model of invasive aspergillosis and found that the Δ*myoB* and Δ*myoE* strains each showed decreased mortality compared to the wild-type strain in this second disease model ($p<0.001$ and $p<0.01$, respectively) (Fig. 4B).

Histopathological examination of murine lungs from mice day +3 after infection demonstrated invasive hyphal growth in the wild-type and in the Δ*myoE* strains, yet little hyphal growth in the

307 Δ*myoB* strain (Fig. 4C). Hematoxylin and eosin staining showed similar inflammation levels for
308 both single deletion strains compared to the wild-type strain (Fig. 4C).

309 The Δ*myoB* strain did not exhibit extensive fungal growth in the murine lungs, but did seem to
310 elicit a pulmonary inflammatory response similar to the wild-type strain by H&E staining.
311 Because H&E staining can be variable based on the different sections of the lung analyzed, we
312 wanted to determine if the Δ*myoB* strain was immunoreactive using a more quantitative assay.
313 To determine this, we collected bronchoalveolar lavage fluid from infected mice three days after
314 infection. We measured the TNF-α released via ELISA and subjected the rest of the BALF to
315 flow cytometry analysis. BALF collected from mice infected with the Δ*myoE* strain did not
316 exhibit a significant difference in TNF-α release compared to that released from the wild-type
317 strain ($p>0.9$); however, those mice infected with the Δ*myoB* strain showed a significant
318 reduction in TNF-α release compared to those infected with the wild-type strain ($p<0.05$) (Figure
319 4D). Cellular analysis revealed that the percentage of leukocytes in the total cell population
320 measured was similar for mice infected with mock and all four strains. The vast majority of
321 leukocytes were either neutrophils or macrophages with macrophages being the primary
322 leukocyte type in mock-infected mice (Figure 4E). The total number of macrophages were
323 similar for mice infected with the wild-type, Δ*myoE* strain or the mock control; however those
324 infected with the Δ*myoB* strain showed statistically more macrophage infiltration compared to
325 the wild-type strain ($p<0.01$). Neutrophil infiltration was highest in mice infected with the wild-
326 type strain while those infected with either mutant strain showed decreased number of
327 neutrophils.

328 **Loss of myosins causes delayed germination and loss of *myoB* results in decreased conidial**
329 **viability.** Due to the conidiation defect and lack of growth of the Δ*myoB* strain in the murine

lungs, we speculated that deletion of *myoB* may result in germination or conidial viability deficiencies. As shown in Fig. 5A, all three myosin deletion strains showed significantly delayed germination compared to the wild-type strain, with the Δ*myoB* Δ*myoE* strain severely delayed. All three deletion strains failed to reach 100% germination.

To directly assess conidial viability, conidia from the wild-type strain and all three myosin deletion strains were stained with bis-(1,3-dibutylbarbituric acid) trimethine oxonol (DiBAC), and carboxyfluorescein diacetate (CFDA) which stain dead and live cells, respectively (34, 35). While the Δ*myoE* strain showed no conidial viability defects, the Δ*myoB* exhibited a greater than 2-fold increase in inviable conidia compared to the wild-type strain ($p<0.05$), shown using complementary stains, suggesting that *myoB* is important for preserving conidial viability (Fig. 5B,C). Based on this result, we attribute that the decreased mortality and fungal burden observed with infection with the Δ*myoB* strain is likely due to reduced conidial viability. Unfortunately, attempts to re-evaluate virulence with equivalent numbers of viable Δ*myoB* conidia, normalized to the number of conidia used for infections with the Δ*myoE* and wild-type strains, was not technically possible due to higher conidial concentration interfering with safe murine intranasal inoculation. The Δ*myoB* Δ*myoE* double deletion strain could not be quantified for conidial viability because the conidia could not be pelleted upon centrifugation. Because conidia were produced in the mutant strains only in the presence of sorbitol, an osmotic stabilizer, we also wanted to determine if harvesting and storing conidia in water had an effect on viability. We harvested and diluted conidia in water or PBS, and then performed the viability staining with DiBAC and CFDA as previously described. Staining revealed that conidia harvested in either water or PBS resulted in no statistically different viability for any strains (Fig S2).

In order to determine if the myosin deletion strains may have defects in the conidial wall surface which could trigger greater immune response or nonviability, we performed TEM on the Δ*myoB* and Δ*myoE* conidia (Fig. 5D). The Δ*myoB* conidia showed an electron dense outer layer that in some instances looked thicker than wild-type strain. This heterogeneity in phenotype was not seen in the wild-type strain. In contrast, the Δ*myoE* conidia generally showed no electron dense outer layer.

DISCUSSION

Myosins are involved in diverse and critical cellular processes, and thus are paramount to understanding fungal growth, septation, and virulence, which may lead to future antifungal targeting. We conducted the first genetic characterization of the class II and class V myosin genes in *Aspergillus fumigatus* (*myoB* and *myoE,* respectively). *myoB* is required for normal septation, as deletion of *myoB* resulted in significant lateral or central joining defects. MyoB also localized transiently to the septa and in rings in the hyphae at presumed sites of septation, consistent with MyoB's known role as part of the actin-myosin ring to form septa (5, 21, 36-38). In contrast to the Δ*myoB* strain in *A. nidulans, A. fumigatus myoB* is dispensible for radial growth, therefore displaying diverse functional contributions within the same genus (5).

Deletion of *myoE* resulted in a significant loss of radial growth, hyperbranching, and loss of hyphal polarity, demonstrating the role of *myoE* in maintaining apical dominance. Class V myosins are known to be vesicle traffickers to the hyphal tip (5, 19, 23, 24), thus the loss of *myoE* likely results in improper trafficking and components necessary for hyphal extension may be diffusing to non-specific areas, causing hyperbranching and loss in polarity. The class V

myosin's role in septation is unknown, but our data implicate a role for *myoE* in maintaining the regular frequency of septation. MyoE under its native promoter localizes stably to every septa, so it is possible that MyoE is serving as a marker for fully-formed septa to modulate the frequency of septation.

A. fumigatus MyoB and MyoE have important roles in conidial production, germination, and conidia viability. Loss of *myoB* resulted in reduced conidial viability and delayed germination. Although most conidia remained viable in the Δ*myoE* strain, conidial germination reached only approximately 50% by 36 hours. The emergence of a germ tube during conidial germination is known to involve polarization proteins as well as the vesicle trafficking system (39-42). Thus, deletion of *myoE* may result in live conidia, but the inability of the conidia to properly establish polarity to initiate germination.

Myosins are also needed for proper cell wall component distribution. The Δ*myoB* Δ*myoE* strain exhibited β-(1,3)-glucan mislocalization throughout the cytoplasm; in contrast, the Δ*myoB* strain exhibited aberrant accumulation of β-(1,3)-glucan only at septal sites, while the Δ*myoE* strain resulted in normal β-(1,3)-glucan localization. In contrast to β-(1,3)-glucan localization, the Δ*myoE* strain exhibited slight accumulation of chitin as small patches that were usually near septa. In *S. cerevisiae*, loss of *myo2* resulted in chitin mislocalization and Myo2p is required to traffic Chs3p, a chitin synthase enzyme, to proper locations (43). Our data indicate that a similar system may be occurring in *A. fumigatus.*

The Δ*myoB* and Δ*myoE* strains resulted in reduced mortality in both *Galleria* and murine models of invasive aspergillosis compared to the wild-type strain. The attenuated virulence of the Δ*myoE* strain is likely due to impaired radial growth, but the Δ*myoB* strain has growth similar to the wild-type strain *in vitro*. Histopathological analyses showed the Δ*myoB* strain grows less

than the Δ*myoE* strain and the wild-type strain in the murine lungs. Significantly lowered conidial germination and viability of the Δ*myoB* strain is most likely the cause of the reduced mortality and fungal burden. While the Δ*myoB* strain exhibits less fungal burden in the murine lungs, the strain still elicits a pulmonary inflammatory response similar to the wild-type strain as seen by H&E staining. We measured TNF-α release of BALF from infected mice three days after infection to determine if an *in vivo* analysis could recapitulate our histopathology results. Mice infected with the Δ*myoB* strain elicited reduced TNF-α release compared to the wild-type, most likely due to the decreased fungal burden at day 3, and Δ*myoE* strains, indicating that the Δ*myoB* strain is not more immunoreactive or the increase in the signal for inflammation precedes day 3 after infection, such as when spores are in contact with lung epithelium, and thus we were not able capture this due to the time course. Cellular analysis of the lung showed that more macrophages were present in mice infected with the Δ*myoB* strain while fewer neutrophils were present in mice infected with either mutant strain compared to the wild-type strain. Neutrophils are primarily responsible for hyphal killing (44) and therefore one would expect to see fewer neutrophils present in those strains that have hyphal defects or are growing less in murine lungs, such as both mutant strains. On the other hand, macrophages are a primary defense against invading conidia (45); therefore, deletion of *myoB* could result in a disorganization of the conidial cell wall that leads to an increase in macrophage infiltration. This is in agreement with the inflammation seen in the H&E staining and the cellular infiltration analysis. TEM analysis revealed that the electron dense outer layer of Δ*myoB* conidia was intact albeit thicker and may have disproportionate cell wall material, aiding in an increase in immune response. On the other hand, TEM of Δ*myoE* conidia revealed the absence of an electron dense outer layer, suggesting

that 1) MyoE is required for its production or 2) deletion of *myoE* reduces the structural rigidity/attachment of this layer, which is detached through vigorous washing and staining.

In conclusion, we have shown the important but distinct roles that class II and class V myosins have in maintaining proper hyphal morphology and disease pathogenesis in *A. fumigatus*. Both the class II myosin (MyoB) and class V myosin (MyoE) are required for septation, conidiation, and conidial germination. MyoB is necessary for proper conidial viability while MyoE is required for radial growth, hyphal polarity, chitin distribution, and virulence. Furthermore, we have demonstrated that class V myosins have a role in septation as has been found in other fungi. Based on these findings, determining the cell wall composition of the conidia of the myosin deletion strains may provide clues leading to the varied immune reactions, and the identification of class V myosin interactants may help reveal its specific role in septation in filamentous fungi.

FUNDING INFORMATION

NIH (grant 1 R01 AI112595-01 to W.J.S.)

NSF (fellowship DGF 1106401 to J.M.V.)

Any opinion, findings, and conclusions expressed in this publication are those of the authors and do not necessarily reflect the views of the National Science Foundation or NIH.

ACKNOWLEDGMENTS

We acknowledge Dr. Andrew Alspaugh's laboratory (Duke University) for helpful technical support and experimental discussion, Michelle Gignac Plue (Duke University) for assistance in

performing transmission electron microscopy, and Dr. Dee Gunn's laboratory (Duke University) for assistance in performing flow cytometry.

REFERENCES

1. **McGoldrick CA, Gruver C, May GS.** 1995. *myoA* of *Aspergillus nidulans* encodes an essential myosin I required for secretion and polarized growth. J Cell Biol **128:**577-587.

2. **Ali MY, Krementsova EB, Kennedy GG, Mahaffy R, Pollard TD, Trybus KM, Warshaw DM.** 2007. Myosin Va maneuvers through actin intersections and diffuses along microtubules. Proc Natl Acad Sci U S A **104:**4332-4336.

3. **Osherov N, Yamashita RA, Chung YS, May GS.** 1998. Structural requirements for in vivo myosin I function in *Aspergillus nidulans*. J Biol Chem **273:**27017-27025.

4. **Steinberg G.** 2007. Hyphal growth: a tale of motors, lipids, and the Spitzenkörper. Eukaryot Cell **6:**351-360.

5. **Taheri-Talesh N, Xiong Y, Oakley BR.** 2012. The functions of myosin II and myosin V homologs in tip growth and septation in *Aspergillus nidulans*. PLoS One **7:**e31218.

6. **Xiang X, Plamann M.** 2003. Cytoskeleton and motor proteins in filamentous fungi. Curr Opin Microbiol **6:**628-633.

7. **Zhang J, Tan K, Wu X, Chen G, Sun J, Reck-Peterson SL, Hammer JA, 3rd, Xiang X.** 2011. *Aspergillus* myosin-V supports polarized growth in the absence of microtubule-based transport. PLoS One **6:**e28575.

8. **Berg JS, Powell BC, Cheney RE.** 2001. A millennial myosin census. Mol Biol Cell **12:**780-794.

9. **Geli MI, Riezman H.** 1996. Role of type I myosins in receptor-mediated endocytosis in yeast. Science **272:**533-535.

10. **Giblin J, Fernandez-Golbano IM, Idrissi FZ, Geli MI.** 2011. Function and regulation of *Saccharomyces cerevisiae* myosins-I in endocytic budding. Biochem Soc Trans **39:**1185-1190.

11. **Lister IM, Tolliday NJ, Li R.** 2006. Characterization of the minimum domain required for targeting budding yeast myosin II to the site of cell division. BMC Biol **4:**19.

12. **Liu X, Osherov N, Yamashita R, Brzeska H, Korn ED, May GS.** 2001. Myosin I mutants with only 1% of wild-type actin-activated MgATPase activity retain essential in vivo function(s). Proc Natl Acad Sci U S A **98:**9122-9127.

13. **Reck-Peterson SL, Tyska MJ, Novick PJ, Mooseker MS.** 2001. The yeast class V myosins, Myo2p and Myo4p, are nonprocessive actin-based motors. J Cell Biol **153:**1121-1126.

14. **Takeshita N, Yamashita S, Ohta A, Horiuchi H.** 2006. *Aspergillus nidulans* class V and VI chitin synthases CsmA and CsmB, each with a myosin motor-like domain, perform compensatory functions that are essential for hyphal tip growth. Mol Microbiol **59:**1380-1394.

15. **Yamashita RA, May GS.** 1998. Constitutive activation of endocytosis by mutation of *myoA,* the myosin I gene of *Aspergillus nidulans*. J Biol Chem **273:**14644-14648.

16. **Goodson HV, Anderson BL, Warrick HM, Pon LA, Spudich JA.** 1996. Synthetic lethality screen identifies a novel yeast myosin I gene (MYO5): myosin I proteins are required for polarization of the actin cytoskeleton. J Cell Biol **133:**1277-1291.

17. **Goodson HV, Spudich JA.** 1995. Identification and molecular characterization of a yeast myosin I. Cell Motil Cytoskeleton **30:**73-84.

18. **Haarer BK, Petzold A, Lillie SH, Brown SS.** 1994. Identification of MYO4, a second class V myosin gene in yeast. J Cell Sci **107 (Pt 4):**1055-1064.

19. **Johnston GC, Prendergast JA, Singer RA.** 1991. The *Saccharomyces cerevisiae* MYO2 gene encodes an essential myosin for vectorial transport of vesicles. J Cell Biol **113:**539-551.

20. **Watts FZ, Shiels G, Orr E.** 1987. The yeast MYO1 gene encoding a myosin-like protein required for cell division. EMBO J **6:**3499-3505.

21. **Bi E, Maddox P, Lew DJ, Salmon ED, McMillan JN, Yeh E, Pringle JR.** 1998. Involvement of an actomyosin contractile ring in *Saccharomyces cerevisiae* cytokinesis. J Cell Biol **142:**1301-1312.

22. **Canovas D, Boyce KJ, Andrianopoulos A.** 2011. The fungal type II myosin in *Penicillium marneffei*, MyoB, is essential for chitin deposition at nascent septation sites but not actin localization. Eukaryot Cell **10:**302-312.

23. **Govindan B, Bowser R, Novick P.** 1995. The role of Myo2, a yeast class V myosin, in vesicular transport. J Cell Biol **128:**1055-1068.

24. **Hammer JA, 3rd, Sellers JR.** 2012. Walking to work: roles for class V myosins as cargo transporters. Nat Rev Mol Cell Biol **13:**13-26.

25. **Woo M, Lee K, Song K.** 2003. MYO2 is not essential for viability, but is required for polarized growth and dimorphic switches in *Candida albicans*. FEMS Microbiol Lett **218:**195-202.

26. **Weber I, Gruber C, Steinberg G.** 2003. A class-V myosin required for mating, hyphal growth, and pathogenicity in the dimorphic plant pathogen *Ustilago maydis*. Plant Cell **15:**2826-2842.

27. **Steinbach WJ, Cramer RA, Jr., Perfect BZ, Asfaw YG, Sauer TC, Najvar LK, Kirkpatrick WR, Patterson TF, Benjamin DK, Jr., Heitman J, Perfect JR.** 2006. Calcineurin controls growth, morphology, and pathogenicity in *Aspergillus fumigatus*. Eukaryot Cell **5:**1091-1103.

28. **Juvvadi PR, Fortwendel JR, Rogg LE, Burns KA, Randell SH, Steinbach WJ.** 2011. Localization and activity of the calcineurin catalytic and regulatory subunit complex at the septum is essential for hyphal elongation and proper septation in *Aspergillus fumigatus*. Mol Microbiol **82:**1235-1259.

29. **Langfelder K, Philippe B, Jahn B, Latge JP, Brakhage AA.** 2001. Differential expression of the *Aspergillus fumigatus* pksP gene detected in vitro and in vivo with green fluorescent protein. Infect Immun **69:**6411-6418.

30. **Lamoth F, Juvvadi PR, Fortwendel JR, Steinbach WJ.** 2012. Heat shock protein 90 is required for conidiation and cell wall integrity in Aspergillus fumigatus. Eukaryot Cell **11:**1324-1332.

31. **Fortwendel JR, Juvvadi PR, Pinchai N, Perfect BZ, Alspaugh JA, Perfect JR, Steinbach WJ.** 2009. Differential effects of inhibiting chitin and 1,3-{beta}-D-glucan synthesis in ras and calcineurin mutants of Aspergillus fumigatus. Antimicrob Agents Chemother **53:**476-482.

32. **Institute CaLS.** 2008. Reference Method for Broth Dilution Antifungal Susceptibility Testing of Filamentous Fungi; Approved Standard-2nd Ed., Wayne, PA.

33. **Steinbach WJ, Benjamin DK, Jr., Trasi SA, Miller JL, Schell WA, Zaas AK, Foster WM, Perfect JR.** 2004. Value of an inhalational model of invasive aspergillosis. Med Mycol **42:**417-425.

34. **Belaish R, Sharon H, Levdansky E, Greenstein S, Shadkchan Y, Osherov N.** 2008. The Aspergillus nidulans cetA and calA genes are involved in conidial germination and cell wall morphogenesis. Fungal Genet Biol **45:**232-242.

35. **Bowman JC, Hicks PS, Kurtz MB, Rosen H, Schmatz DM, Liberator PA, Douglas CM.** 2002. The antifungal echinocandin caspofungin acetate kills growing cells of Aspergillus fumigatus in vitro. Antimicrob Agents Chemother **46:**3001-3012.

36. **Hill TW, Jackson-Hayes L, Wang X, Hoge BL.** 2015. A mutation in the converter subdomain of *Aspergillus nidulans* MyoB blocks constriction of the actomyosin ring in cytokinesis. Fungal Genet Biol **75:**72-83.

37. **Mulvihill DP, Hyams JS.** 2003. Role of the two type II myosins, Myo2 and Myp2, in cytokinetic actomyosin ring formation and function in fission yeast. Cell Motil Cytoskeleton **54:**208-216.

38. **Song B, Li HP, Zhang JB, Wang JH, Gong AD, Song XS, Chen T, Liao YC.** 2013. Type II myosin gene in *Fusarium graminearum* is required for septation, development, mycotoxin biosynthesis and pathogenicity. Fungal Genet Biol **54:**60-70.

39. **d'Enfert C.** 1997. Fungal Spore Germination: Insights from the Molecular Genetics of *Aspergillus nidulans* and *Neurospora crassa*. Fungal Genet and Biol **21:**163-172.

40. **Harris SD.** 2006. Cell polarity in filamentous fungi: shaping the mold. Int Rev Cytol **251:**41-77.

552 41. **Harris SD, Momany M.** 2004. Polarity in filamentous fungi: moving beyond the yeast
553 paradigm. Fungal Genet Biol **41:**391-400.
554 42. **Momany M.** 2002. Polarity in filamentous fungi: establishment, maintenance and new
555 axes. Curr Opin Microbiol **5:**580-585.
556 43. **Santos B, Snyder M.** 1997. Targeting of chitin synthase 3 to polarized growth sites in
557 yeast requires Chs5p and Myo2p. J Cell Biol **136:**95-110.
558 44. **Park SJ, Mehrad B.** 2009. Innate immunity to Aspergillus species. Clin Microbiol Rev
559 **22:**535-551.
560 45. **Philippe B, Ibrahim-Granet O, Prevost MC, Gougerot-Pocidalo MA, Sanchez Perez**
561 **M, Van der Meeren A, Latge JP.** 2003. Killing of Aspergillus fumigatus by alveolar
562 macrophages is mediated by reactive oxidant intermediates. Infect Immun **71:**3034-3042.

563

564 **Fig.1.** Myosins are required for proper hyphal and septal morphology. (A) Deletion of *myoB*
565 resulted in white colonies with wild-type (WT) radial growth. Deletion of *myoE* resulted in
566 white, compact colonies. Conidia (10^4) were spotted onto GMM agar and incubated for 5 days at
567 37°C. Single deletion of *myoB* resulted in β-(1,3)-glucan mislocalization and deletions of *myoB*
568 or *myoE* resulted in chitin mislocalization. Conidia (10^4) were inoculated into 5 ml GMM on
569 sterile coverslips for 18 h at 37°C. Coverslips were stained with aniline blue to stain β-glucan or
570 calcofluor white to stain chitin and were visualized using fluorescent microscopy. White
571 arrowhead indicates normal septa, dotted white arrows indicate β-(1,3)-glucan mislocalization,
572 and solid white arrows indicate chitin mislocalization. (B) Strains with deletions of both *myoB*
573 and *myoE* result in hyperbranching and β-(1,3)-glucan patches throughout the hyphae. (C)
574 MyoB is required for proper septum formation. Deletion of *myoB* resulted in malformed, thicker

septa than wild-type. Septa were visualized using transmission electron microscopy (TEM). Black arrowhead points to normal septa and black dotted arrows indicate aberrant septa in the *myoB* deletion strain. (D) Strains harboring a deletion of *myoE* resulted in a significant radial growth defect. Conidia (10^4) were spotted onto GMM agar and incubated for 5 days at 37°C. Radial growth was measured every 24 h.

Fig 2. Myosin deletion strains are sensitive to anti-cell wall agents. (A) Deletion of *myoB* resulted in increased sensitivity to the β-(1,3)-glucan synthase inhibitor, caspofungin (CSP; 1 μg/ml) but did not abolish paradoxical growth at 4 μg/ml CSP on plates. Deletion of both *myoB* and *myoE* resulted in increased sensitivity to both CSP and the chitin synthase inhibitor, nikkomycin Z (NikZ). Conidia (10^4) were grown on GMM supplemented with the appropriate anti-cell wall drugs for 5 days at 37°C. (B) In liquid media, deletion of *myoB* or *myoE* resulted in increased sensitivity to caspofungin but only the Δ*myoB* strain exhibited a loss of paradoxical growth. The minimum effective concentration (MEC) of caspofungin for the Δ*myoB* strain was 0.25 μg/ml and for the Δ*myoE* strain was 0.125 μg/ml. Conidia were grown in RPMI supplemented with the appropriate concentrations of caspofungin for 48 h at 37°C.

Fig 3. Localization of MyoB and MyoE. **(A)** MyoB localizes in rings in the hyphae. Arrow indicates ring structure. **(B)** MyoE localizes to the fully-formed septa as two discs on either side of it (top panels). MyoE localizes to the hyphal tip and in-dot like structures throughout the hyphae (bottom panels). Insets are close-ups of where arrow is located. Arrows indicate hyphal tip and septa localization.

597

598 **Fig 4.** Effect of *myoB* and *myoE* deletion on virulence in the invertebrate host, *Galleria*
599 *mellonella* and in a murine model of invasive aspergillosis. (A) Conidia (5 x 10^6) were
600 inoculated into invertebrate host, *Galleria mellonella* larvae and survival was scored every 24 h
601 for 5 days. (B) Effect of *myoB* or *myoE* deletion on virulence in a persistently immunosuppressed
602 murine model. Mice were immunosuppressed with cyclophosphamide and triamcinolone
603 acetonide prior to infection. Conidia (4 x 10^6) were inoculated into mice intranasally and survival
604 was scored every 24 h up to 14 d. (C) Histopathological examination of the murine lungs 3 days
605 after infection showed little fungal burden in the Δ*myoB* strain while the wild-type and Δ*myoE*
606 strains showed similar fungal burden by Gomori methenamine silver stain (GMS) (top panels).
607 Inflammation was similar in the wild-type and single deletion strains by hematoxylin and eosin
608 (H&E). (D) BALF from infected mice was used to determine TNF-α released by ELISA. Mice
609 infected with the Δ*myoB* strain released significantly less TNF-α than wild-type or Δ*myoE*. (E)
610 BALF from infected mice was used for leukocyte analysis by flow cytometry. *indicates
611 significance of $p<0.05$ using an unpaired t-test (compared to WT).

612

613 **Fig 5.** Myosins are required for conidial germination. (A) Conidia (~100) were inoculated into
614 GMM, grown at 37°C, and quantified as germinated or not using a Nikon Diaphot Phase
615 Contrast microscope at the indicated time points. (B,C) Conidia were stained with (B) bis-(1,3-
616 dibutylbarbituric acid) trimethine oxonol (DiBAC) or (C) carboxyfluorescein diacetate (CFDA)
617 and quantified by fluorescent microscopy. (D) Deletion of *myoB* results in conidia with a thicker
618 electron-dense outer layer while deletion of *myoE* results in conidia lacking this layer. Conidia

were visualized by TEM. * indicates significance of $p<0.05$ using an unpaired t-test (compared to WT).

Table 1. Strains used in this study

Strain	Parent Strain	Genotype	Reference
akuB^{KU80}	CEA17	Wild-type	CBS144-89 (5)
akuB^{KU80} *pyrG*$^{-}$	CEA17 *pyrG*$^{+}$	*pyrG*	(43)
ΔmyoB	*akuB*^{KU80} *pyrG*$^{-}$	*ΔmyoB::pyrG*	This study
ΔmyoE	*akuB*^{KU80} *pyrG*$^{-}$	*ΔmyoE::pyrG*	This study
ΔmyoB ΔmyoE	*ΔmyoB*	*ΔmyoB::pyrG ΔmyoE::ble*	This study
myoB-egfp	*akuB*^{KU80}	*myoB::myoBpromo-myoB-egfp-hph*	This study
myoE-egfp	*akuB*^{KU80}	*myoE::myoEpromo-myoE-egfp-hph*	This study

Figure 1

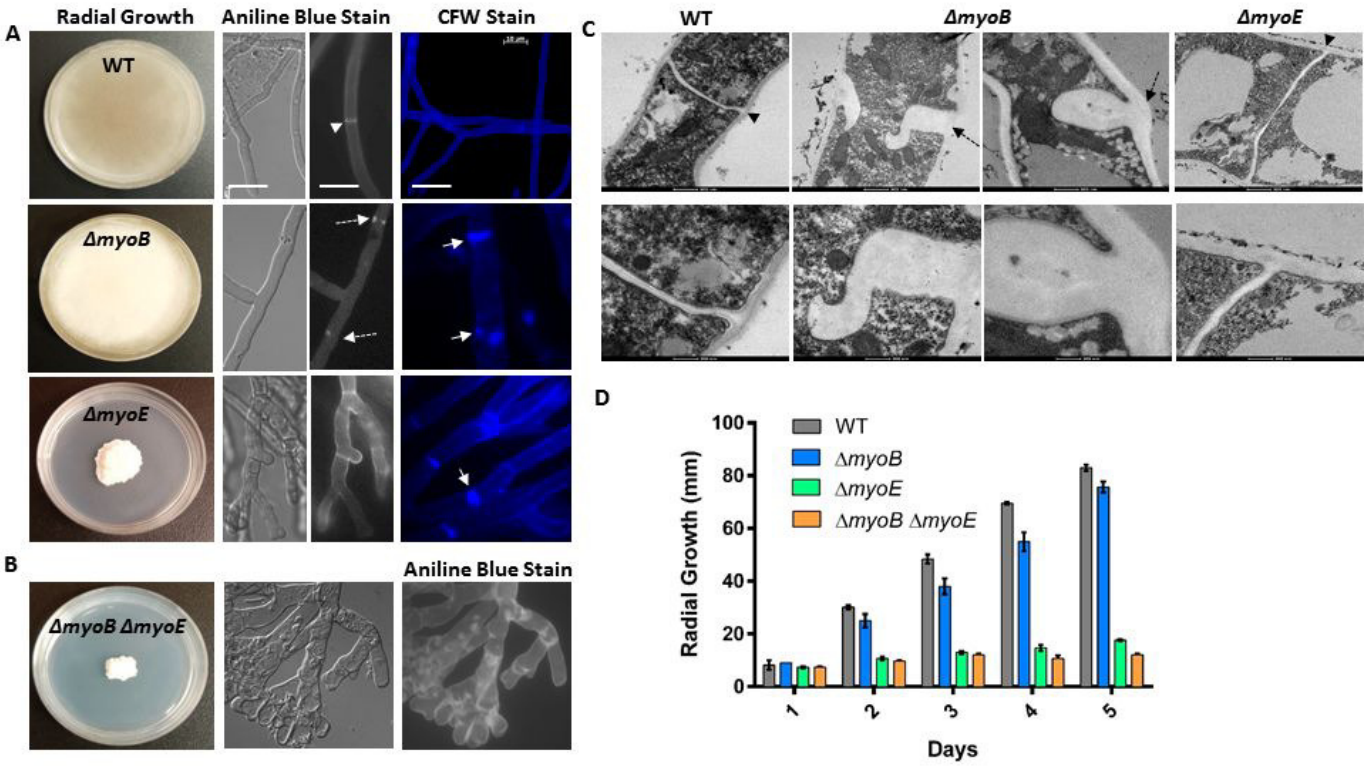

Figure 2

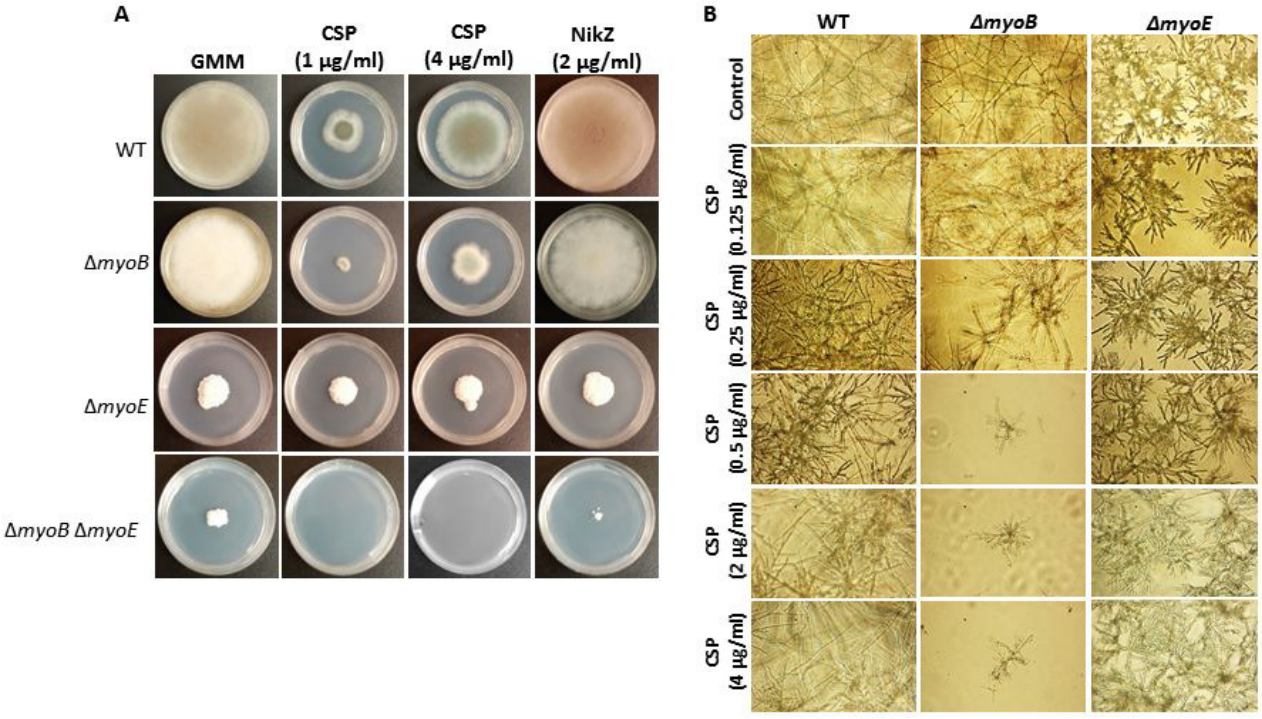

Figure 3

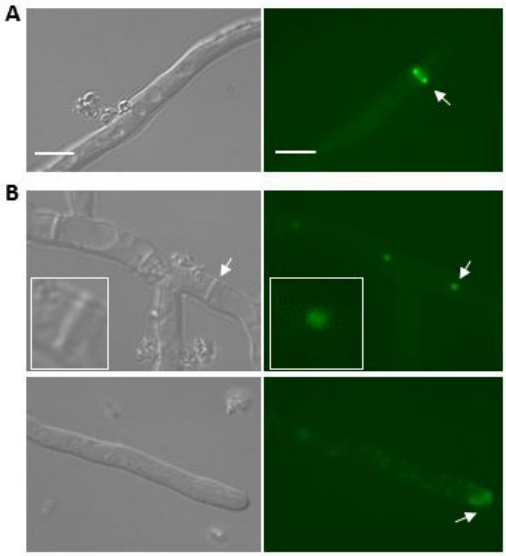

Figure 4

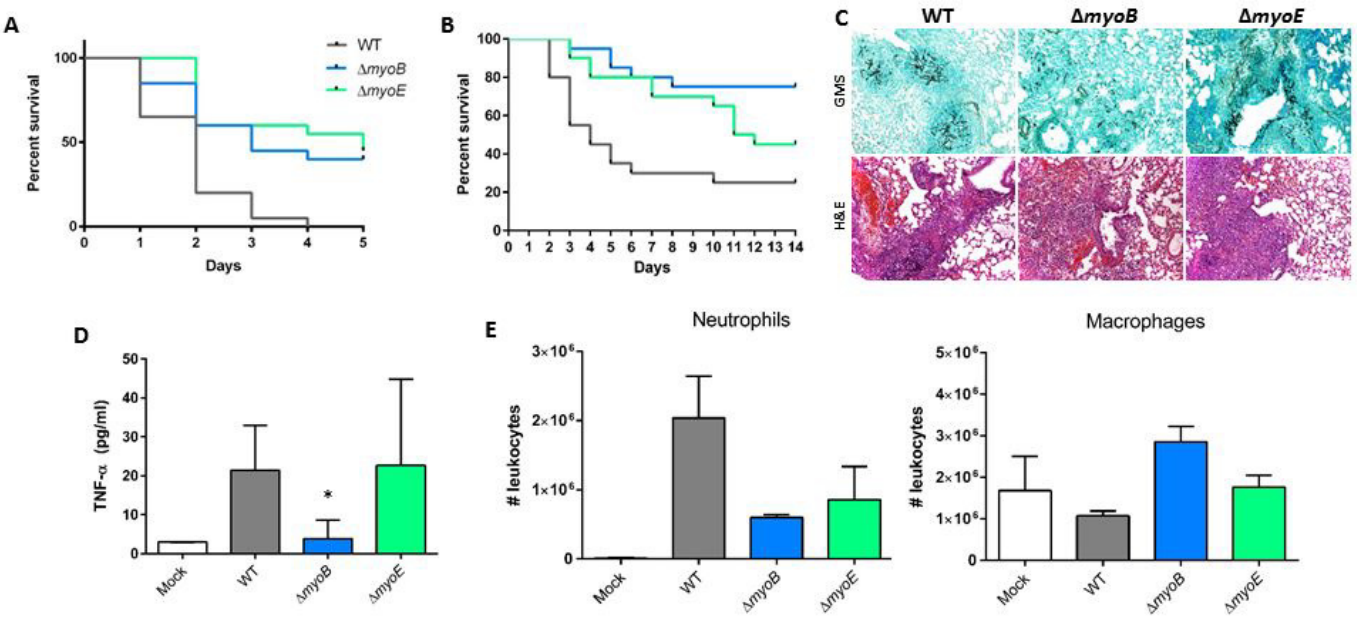

Figure 5